SANDIA REPORT

SAND2010-7425
Unlimited Release
Printed November 2010

Preliminary Studies of Tunnel Interface Response Modeling Using Test Data from Underground Storage Facilities

Steven R. Sobolik and Lewis C. Bartel
Energy, Resources, and Systems Analysis Center
Sandia National Laboratories
P.O. Box 5800
Albuquerque, New Mexico 87185-0751

Prepared by
Sandia National Laboratories
Albuquerque, New Mexico 87185 and Livermore, California 94550

Sandia National Laboratories is a multi-program laboratory managed and operated by Sandia Corporation, a wholly owned subsidiary of Lockheed Martin Corporation, for the U.S. Department of Energy's National Nuclear Security Administration under contract DE-AC04-94AL85000.

Issued by Sandia National Laboratories, operated for the United States Department of Energy by Sandia Corporation.

Available to DOE and DOE contractors from
U.S. Department of Energy
Office of Scientific and Technical Information
P.O. Box 62
Oak Ridge, TN 37831

Telephone: (865) 576-8401
Facsimile: (865) 576-5728
E-Mail: reports@adonis.osti.gov
Online ordering: http://www.osti.gov/bridge

Available to the public from
U.S. Department of Commerce
National Technical Information Service
5285 Port Royal Rd.
Springfield, VA 22161

Telephone: (800) 553-6847
Facsimile: (703) 605-6900
E-Mail: orders@ntis.fedworld.gov
Online order: http://www.ntis.gov/help/ordermethods.asp?loc=7-4-0#online

SAND2010-7425
Unlimited Release
Printed November 2010

Preliminary Studies of Tunnel Interface Response Modeling Using Test Data from Underground Storage Facilities

Steven R. Sobolik and Lewis C. Bartel
Energy, Resources, and Systems Analysis Center
Sandia National Laboratories
P.O. Box 5800
Albuquerque, New Mexico 87185-0751

ABSTRACT

In attempting to detect and map out underground facilities, whether they be large-scale hardened deeply-buried targets (HDBT's) or small-scale tunnels for clandestine border or perimeter crossing, seismic imaging using reflections from the tunnel interface has been seen as one of the better ways to both detect and delineate tunnels from the surface. The large seismic impedance contrast at the tunnel/rock boundary should provide a strong, distinguishable seismic response, but in practice, such strong indicators are often lacking. One explanation for the lack of a good seismic reflection at such a strong contrast boundary is that the damage caused by the tunneling itself creates a zone of altered seismic properties that significantly changes the nature of this boundary. This report examines existing geomechanical data that define the extent of an excavation damage zone around underground tunnels, and the potential impact on rock properties such as P-wave and S-wave velocities. The data presented from this report are associated with sites used for the development of underground repositories for the disposal of radioactive waste; these sites have been excavated in volcanic tuff (Yucca Mountain) and granite (HRL in Sweden, URL in Canada). Using the data from Yucca Mountain, a numerical simulation effort was undertaken to evaluate the effects of the damage zone on seismic responses. Calculations were performed using the parallelized version of the time-domain finite-difference seismic wave propagation code developed in the Geophysics Department at Sandia National Laboratories. From these numerical simulations, the damage zone does not have a significant effect upon the tunnel response, either for a purely elastic case or an anelastic case. However, what was discovered is that the largest responses are not true reflections, but rather re-radiated Stoneley waves generated as the air/earth interface of the tunnel. Because of this, data processed in the usual way may not correctly image the tunnel. This report represents a preliminary step in the development of a methodology to convert numerical predictions of rock properties to an estimation of the extent of rock damage around an underground facility and its corresponding seismic velocity, and the corresponding application to design a testing methodology for tunnel detection.

ACKNOWLEDGEMENTS

The authors would like to thank Leiph Preston for his assistance and to David Holcomb and Greg Elbring for their review and support of this work.

TABLE OF CONTENTS

LIST OF FIGURES

LIST OF TABLES

1. INTRODUCTION

1.1 OBJECTIVE

In attempting to detect and map out underground facilities, whether they are large-scale hardened deeply-buried targets (HDBTs) or small-scale tunnels for clandestine border or perimeter crossing, seismic imaging using reflections from the tunnel interface has been seen as one of the better ways to both detect and delineate tunnels from the surface. The large seismic impedance contrast at the tunnel/rock boundary should provide a strong, distinguishable seismic response, but in practice, such strong indicators are often lacking. One explanation frequently offered for the lack of a good seismic reflection at such a strong contrast boundary is that the damage caused by the tunneling itself creates a zone of altered seismic properties that significantly changes the nature of this boundary. The character and extent of the altered zone, usually referred to as an excavation damaged zone (EDZ), is known to depend on the competence of the geologic media and the method of excavation. There are several potential mechanisms by which tunnel excavation may impact wave propagation in the host rock:

- creation of large fractures (or enhancement of existing fractures);
- rubblization of the host rock;
- creation of microfractures
- localized desaturation of moisture into the tunnel; and
- significant stress/strain changes around the tunnel.

A literature search conducted to locate experimental studies of damage around excavation zones yielded one comprehensive examination of characteristics of the EDZ in several geologic media (Tsang, et al., 2005), and relevant data from several underground studies of potential nuclear waste repositories, with some experimental studies of the effect of the EDZ on seismic wave measurements in the tunnel vicinity. However, no experimental study was found that correlated EDZ effect on seismic wave propagation to remote tunnel detection.

In response to the need to detect underground facilities, the authors proposed a study to examine the geomechanical changes caused by tunneling and the consequent effect on seismic velocities, to determine whether this gives rise to the lack of strong seismic reflections. The first portion of this study, described in this report, utilized available experimental data from several underground exploratory facilities to quantify the effect of different construction methods in terms of radial extent of the EDZ in certain geologic media, and the change in specific rock mechanical properties. These quantities were then used as input to a parallelized version of the time-domain finite-difference seismic wave propagation code developed in the Geophysics Department at Sandia National Laboratories, which is used to model P-wave and S-wave seismic behavior for given geometries. Using a combination of data and seismic wave analyses, the development of a methodology for the case of tunnel construction damage will begin, focusing on calculation of damage zone thickness based on geologic medium and construction method, and correlation of these effects to seismic measurements. It is anticipated that this preliminary effort will be used as a precursor to a more extensive modeling effort to simulate boring and drill-and-blast excavation methods using the CTH computational dynamics code. The cutting-edge aspect is the

development of methodology to convert numerical predictions to an estimation of the extent of rock damage around an underground facility and its corresponding impact on seismic response.

Two sets of data relating to underground facilities in geologic media were used for this report. One set of data come from the study of a site at Yucca Mountain, Nevada, as a potential site for the permanent storage of radioactive waste. Yucca Mountain consists of several layers of volcanic tuff, each layer varying in its degree of crystalline welding, porosity, and fracturing. The second set of data comes from two similar sites set in granitic rock in Sweden and Canada. Geomechanical and seismic data from these sites have been used to estimate the radial extent of the EDZ and the corresponding change in rock mass modulus and seismic wave velocities.

1.2 REPORT ORGANIZATION

This report is organized in the following fashion: Section 2 describes the definition of an excavation damage zone, how that might relate to seismic tunnel detection, and the observed extent of the EDZ in several geologic media. This section also details the relevant available data for underground facilities in two geologic media: the Drift Scale Test at Yucca Mountain, Nevada, which was built in welded volcanic tuff; and test facilities for potential nuclear waste repository in Sweden and Canada built in granitic rock. Section 3 describes the seismic analysis model using data from Yucca Mountain, including the conceptual model, material properties, and damage criteria used for the analyses. The conclusions drawn from the simulations are listed in Section 4. The report concludes with a list of cited references in Section 5.

2. CHARACTERIZATION OF THE EDZ

As a part of a greater international effort to identify and characterize potential sites for permanent underground disposal of radioactive waste, Tsang et al. (2004) conducted a study to define, describe, and quantify the effects of the excavation of a tunnel in a host rock, and the long-term consequences of those effects on the isolation of radioactive waste from the accessible environment. They define an excavation damaged zone (EDZ) as a zone with hydromechanical and geochemical modifications inducing significant changes in flow and transport properties. These changes can, for example, include one or more orders of magnitude increase in flow permeability. Obviously, because their report evaluates geologic media for radioactive waste disposal, their definition emphasizes effects on hydrology and radionuclide transport; however, a change in fracture density also results in changes in rock mass modulus and seismic wave velocity. Tsang et al. (2005) also define an excavation disturbed zone (EdZ) as a zone with hydromechanical and geochemical modifications, without major changes in flow and transport properties.

During excavation of a tunnel, damage to the surrounding host rock may occur from three mechanisms: the excavation method itself (tunnel boring machine (TBM), drill-and-blast, alpine miner, etc.); mechanical changes caused by stress redistribution around the newly excavated opening; and back-pressure on rock deformation by emplacement of drift support (which is not considered in this report). Table 1 summarizes the key processes, parameters, and technical issues for the formation of an EDZ during excavation. These processes are listed by four rock types: crystalline rock (which would include volcanic tuff and granitic rock), rock salt, indurated clays, and plastic clays. For crystalline rock, the expected radial extent of the EDZ depends on the construction method: up to 0.75 m from drill-and-blast, and much less using a TBM. (The radial extent would be expected to be greater for a more porous crystalline rock such as volcanic tuff; this expectation is confirmed in subsequent sections.) The stress redistribution around the tunnel after excavation has a greater influence on the extent of the EDZ, creating an EDZ as much as one tunnel radius from the wall. One other important observation is that newly created fractures tend to be oriented parallel to the tunnel, creating anisotropic conditions for both hydraulic permeability and rock mass modulus. Tsang et al. report a change in permeability in the EDZ of 2-3 orders of magnitude. Permeability is proportional to the fracture spacing and the cube of fracture aperture, and typically an order of magnitude increase in fracture permeability corresponds to a 10-20% reduction in rock mass modulus.

Two sets of data relating to underground facilities in geologic media were used for this report. The first data come from the study of a potential radioactive waste repository in Yucca Mountain, Nevada, in welded, lithophysal volcanic tuff. The second set of data is compiled from two repository sites in Sweden and Canada based in granitic rock. Extensive data exist for these sites for mechanical changes to the host rock: observation of new fracture after excavation, measurement of in situ rock mass modulus, seismic velocity measurements, and acoustic event measurements. These data were used in a preliminary effort to determine their effect on mechanical seismic properties and the resulting impact on seismic detection measurements. Due to time constraints, only the Yucca Mountain data were used for a numerical simulation of seismic wave detection for this report.

Table 1. Comparison of processes, parameters, and issues for EDZ in different rock types: excavation stage (construction damage; stress redistribution) (from Tsang et al., 2005)

	Crystalline Rock	Rock Salt	Indurated Clay	Plastic Clay
Processes and Events	• Excavation procedure giving rise to EDZ – Drill-and-blast: Δk ~2–3 om; thickness ~10–75 cm – Tunnel Boring Machine: Δk ~1 om; thickness ~1 cm • Stress redistribution due to opening, causing tension, compression and shear in different parts around the drift – Δk (axial) ~1 om – Δk (radial) magnitude reduces to 1/5 original – Extent: up to 2-3 m beyond wall of a 5-m drift; thicker on floor than side and roof of drift	• Effects of excavation procedures are less significant. • Stress redistribution due to opening, causing tension, compression and shear in different parts around the drift • Microcracking at locations where dilatancy criterion is exceeded • Permeability increase with opening of microcracks; • EDZ extends 0.5 m into wall and 1.5 m into floor; Δk is 4–5 om and is anisotropic	• Stress redistribution giving rise to strongly anisotropic, deviatoric compression and/or tensile stresses, causing (a) tensile and shear fracturing along bedding planes and (b) vertical extensional or tensile fracturing in rock near side walls • Data show vertical fracture in drift walls: 10–30/m within the first m; 5–10/m in the 1-2 m and ~0/m beyond 2 m • Generally, EDZ is one drift radius from drift wall with Δk up to ~6 om • Transient pore-pressure dissipation	• Stress release at excavation (stress redistribution) leading to contractant and dilatant processes with induced fracturing; • Undrained behaviour expected in the short term; • Dilation inducing suction and pseudo-strength increase; • Shear behaviour also expected (slick and sliding); • Curved fractures with apex at front end of 4.8 m drift, extending several metres from the rock wall, but fractures closed beyond 1 m; • Evidence of extension fractures (relay fractures) for ~4 m on front of excavation; • Piezometric response far ahead of excavation front (60 m), but negligible Δk
Property and Design Parameters	• *In situ* stress, including stress anisotropy; • Rock strength (failure initiation strength); • Initial *in situ* fracture network (density and orientations), • Orientation of drift relative to principal stress directions, size and shape of drifts; • Excavation sequence, quality assurance and control.	• State of stress (depth of repository); • Dilatancy, healing and creep properties of the salt • Geometry of drift; • Procedure for rock support immediately following excavation • Lithologic heterogeneity	• Rock property parameters; anisotropy (bedding planes) • *In situ* stress state, including stress anisotropy • Drift orientation relative to bedding plane directions and to fracture directions • Drift (gallery) shape, • Methods of excavation with emplacement of support, • Moisture content in rock and transient pore pressure	• *In situ* stress-strength ratio; • Excavation and lining installation procedure to limit wall convergence • Parameters related to shear and extensional fracturing • Presence of bedding planes or planes of weakness. • Excavation shape and initial stress state
	Crystalline Rocks	**Rock Salt**	**Indurated Clays**	**Plastic Clays**
Some Technical Factors	• Difference in EDZ developed along part of the drift away from and the part near to fracture zones intercepting the drift. More studies of EDZ at drift-fracture intersections and its role may be useful. • EDZ at tunnel intersections may need special considerations • Some apparent differences in results from Stripa, Grimsel (FEBEX), Aspo and Pinawa URL; perhaps due to different *in situ* stress, drift size and drift orientation and fracture network in rock, as well as different excavation methods.	• Deviatoric stress can increase air k up to 4 om by inducing new micro cracks • Δk - Δϕ relationship shows two regimes: – Initial ϕ opening with large Δk of 4 to 5 om by increasing fracture connectivity – Later ϕ increase corresponding to crack opening after network connectivity is established, with Δk of ~2 om.	• Medium characterized by dependence on moisture content: low moisture case corresponds to harder rock and high case corresponds to ductile (soft) behaviour • Role of structures (bedding planes), weathering (drying), dissolution and oxidation; • Nonlinear stress-strain behaviour dependent on stress level, suction (water content) and weathering conditions; • Stress and strain localization: onset and propagation of discontinuity; effect of heterogeneity.	• Naturally occurring fractures are found in outcrops with spacing 0.5 to several metres; mostly extensional fractures with a small part shear fractures. However, they are not seen at depth. Confining pressure, as well as moisture content, is reason for absence of fractures.

NOTE: EDZ = excavation-disturbed/damaged zone; Δk = increase in permeability k; Δϕ = change in porosity; om = orders of magnitude

2.1 Yucca Mountain Site – Welded Volcanic Tuff

Yucca Mountain, Nevada, has been identified by the U.S. Department of Energy (DOE) as a potential site for the permanent storage of radioactive waste. Yucca Mountain consists of several layers of volcanic tuff, each layer varying in its degree of crystalline welding, porosity, and fracturing. The site has undergone extensive scientific investigation since 1980. The primary tunnel in Yucca Mountain, the Exploratory Studies Facility (ESF), was constructed in the mid-

1990s. The ESF was constructed using a tunnel boring machine (TBM). After construction of the ESF, several test alcoves were excavated. These alcoves were excavated using one or both of two methods, alpine mining, and drill-and-blast excavation. The major underground experiment in the ESF was the Drift Scale Test (DST), a 50-m long, 5.5-m diameter Heated Drift in which the heat input from radioactive waste emplacement was simulated using canister and in-rock heaters, heating the tunnel and surroundings to a maximum temperature of 250°C for four years. Several sets of relevant data from the DST were used for determining the extent of the EDZ (Wagner et al., 2002): an in situ plate loading test that measured rock mass modulus, visual inspection of fracture formation during construction; fracture maps from the Heated Drift; and displacement data taken from a mine-by drift during drift construction that can be used to estimate the extent of fracture damage. In addition, several measurements of saturation were taken during the heating and cooldown phases of the DST, and acoustic instrumentation recorded microseismic events as well; unfortunately, there was not enough correlation to determine a relationship between change in saturation and wave velocity. Thus, the DST data can be used to evaluate two mechanisms by which tunnel excavation may impact the wave propagation of the host rock: the creation of fractures and/or enhancement of existing fractures during excavation; and the redistribution of stress and strain after tunnel excavation. The resulting changes in bulk modulus can be converted to changes in wave velocities, which would be supplied as input to seismic simulation codes to see whether changes in seismic velocities are sufficient to mute the tunnel reflections.

The relevant data from the Yucca Mountain Project (YMP) were obtained from the following tunnels and alcoves:

- Exploratory Studies Facility (ESF), the 5.5-m diameter main tunnel in Yucca Mountain;
- Experimental Alcove 2, near the ESF North Portal, located in upper and middle nonlithophysal tuff;
- Alcove 5, Thermal Test Facility (TTF), location of Access Observation Drift (AOD), Connecting Drift (CD), and Heated Drift (HD), which housed the Drift Scale Test (DST) and Plate Loading Test (PLT); the HD is 5.5m in diameter, under approximately 175 m of overburden. A plan view of the test facilities in Alcove 5 is shown in Figure 1, and a diagram of the instrumentation boreholes in the vicinity of the DST in shown in Figure 2.

Yucca Mountain is composed of several layers of volcanic tuff with varying degrees of lithophysal porosity, fracturing, welded crystalline structure, and rock quality. Most of the YMP facilities are located in the stratigraphic layer TSw2, the Topopah Springs middle nonlithophysal tuff. Most of Alcove 2 and all of Alcove 5 are in TSw2.

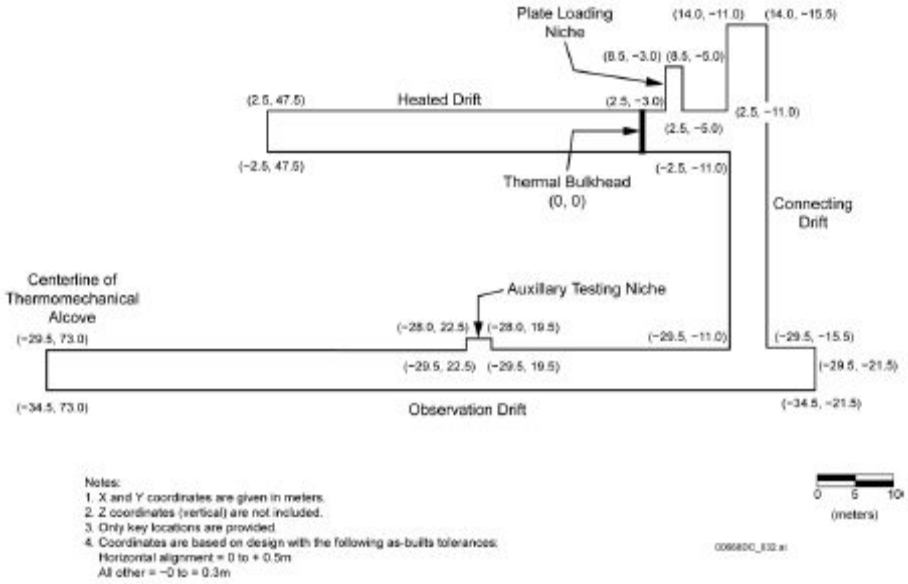

Figure 1. DST As-Built Plan View with Two-Dimensional Coordinates of Key Locations (Wagner et al., 2002).

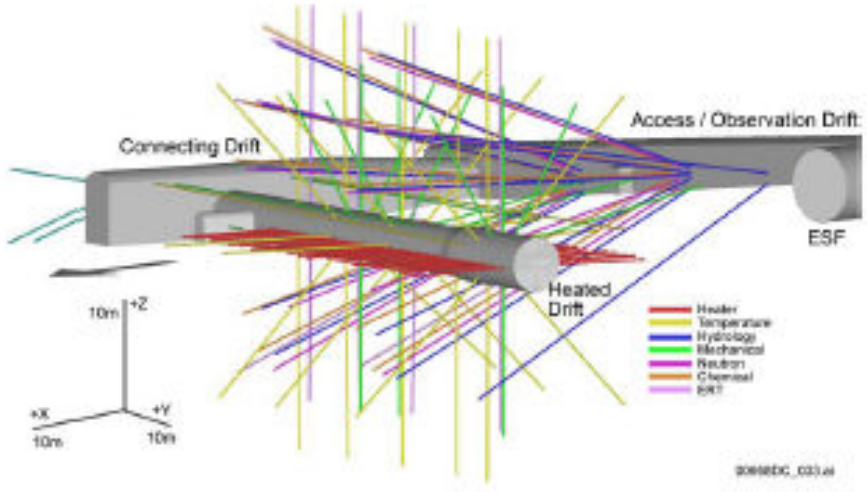

Source: DTN: MO0002ABBLSLDS.000 [DIRS 147304].

NOTE: Schematic is prepared from coordinates based on an origin located at the center of the heated drift bulkhead.

Figure 2. Drifts and Boreholes of the DST (Wagner et al., 2002).

There were several sets of data from YMP test areas and samples relevant to the investigation of seismic wave detection of tunnels. These data include the following items.

1. Intact rock thermomechanical properties

Prior to underground testing, several samples of TSw2 were obtained for laboratory mechanical and thermal testing. The following laboratory measurements were obtained for intact rock properties for TSw2:

- Static Young's Modulus of TSw2 (DST) rock – 36.8 GPa ± 3.5 (YMP, 1997b)
- Static Poisson's Ratio 0.201 +- 0.040 (YMP, 1997b)
- Density 2270 kg/m^3 (YMP, 1997b)
- Unconfined Compressive Strength 176.4 MPa ± 65.8 (YMP, 1997b)
- Thermal expansion between 25°C and 50°C: 7.47 μm/m/°C (YMP, 1997c)

2. Rock mass modulus

To determine potential changes in the rock mass modulus resulting from the excavation of the Heated Drift and from potential thermally induced closure of fractures, a plate loading niche was constructed near the DST, as shown in figure 1. The niche was constructed such that one side would be near ambient temperature and the other side affected by the heat generated by the nearby DST. Rock mass modulus, a parameter of significance to the Yucca Mountain geomechanics program, was calculated using data gathered from the Plate Loading Test (PLT). The rock mass modulus differs from the standard Young's modulus in that the presence of fractures in the host rock affects the amount of deformation under an applied load. A series of three tests were performed, in 1998, 2000, and 2003. Using pressure and displacement test data from the latter two tests, and implementing the calculation method defined in ASTM 4394, the following values were obtained for rock mass modulus on the ambient side of the niche:

- From 10/17/2000 test (YMP, 2000): Rock mass Young's modulus 12.6 GPa, intact rock modulus 27.4 GPa
- From 4/30/2003 test (YMP, 2003): Rock mass Young's modulus 11.4 GPa, intact rock modulus 27.3 GPa

The resulting 55-60% decrease in modulus from intact to rock mass results in an expected decrease in P-wave velocity of approximately 33%. It is unclear whether this decrease is due entirely to fracture formation during excavation, or whether the additional stress redistribution during test setup and the heating phase also contributed.

3. In situ seismic velocity measurements

In support of an infiltration experiment to study hydrological behavior between two drifts at Yucca Mountain, a series of seismic tomographic measurements were conducted in the TSw2 rock (Descour et al., 2001). The measurements were conducted between Niche 3 in ESF, and Alcove 8 in the overlying Enhanced Characterization of the Repository Block (ECRB) cross-drift. The measurements were used to assess the lithologic structures between the two access drifts, and to use the velocity signatures to characterize the rock prior to the infiltration experiment. The tomographic measurements indicated three distinct zones in the rock between the drifts, with slightly varying values (±15%) for P-wave and S-wave velocities. The results also seemed to indicate that lower velocities in one zone may correspond to higher permeability due to the fractured rock structure. The average velocities obtained for TSw2 were the following values:

- V_P=3000 m/s; V_S=1800 m/s

4. Rock mass quality

Rock mass quality parameters were developed for all the stratigraphic layers in Yucca Mountain through which the ESF traverses. Table 2 is a summary of the rock mass quality indices for TSw2 (Lin et al., 1995).

Table 2. Rock mass quality indices for TSw2 (from Lin et al., 1995).

Rock Mass Quality Category	Frequency of Occurrence (%)	Q Value	RMR Value
1	5	0.30	51
2	20	0.65	56
3	40	1.91	58
4	70	3.75	63
5	90	8.44	67

5. Measure displacement during excavation of the Heated Drift

Displacement in the Heated Drift walls during construction and test setup were measured by mine-by multi-point borehole extensometers (MPBXs). The closest distance of any MPBX anchor to the HD wall is about 2 m. Anchors range from 2 to 11 meters from the HD wall. Displacements were measured relative to a collar approximately 28 meters from the HD wall. Measurements began at t=-375 days (375 days before the heat was turned on); tunnel construction occurred between t=-351 to t=-302 days. The following observations can be made from the MPBX data:

- SDM-MPBX-1 (the extensometer closest to the open end of the Heated Drift) shows steady increase in length throughout the HD construction period, with occasional "slips" (sudden changes in displacement) for individual anchors, but no slips affecting multiple anchors at the same time. The displacements are shown in Figure 3. Maximum displacement is about 0.25 mm over 25 m.
- SDM-MPBX-2 shows minimal, steady decrease in length for the five anchors closest to the HD, with most eventually reaching about -0.12 mm displacement, and anchor 1 (the closest to the HD) about -0.25 mm. Anchor 6, which is the furthest from the HD, experiences a significant increase at the time of the invert blasting near the location of MPBX-1, and two smaller jumps at the next two blasting times, up to a maximum increase of about 0.30 mm, before also steadily decreasing to about 0.20 mm at DST startup. The displacements are shown in Figure 4.
- SDM-MPBX-3 shows a similar minimal, steady decrease in length as MPBX-2 with the addition of two significant slip events at 193 and 70 days before DST startup. The slip events do not seem to correlate with known construction activity events. The total decrease in length of the extensometer ranges from -0.19 to -0.35 mm. The displacements are shown in Figure 5.

The magnitudes of these displacements are possibly explained by thermal expansion, as the rock temperature was about 24°C, whereas the air temperature in the drifts was about 32°C. Whatever the reason, an alteration of 0.30 mm over a 2-m thickness indicates a change in

fracture and stress characteristics in the host rock significant enough to potentially have an effect on the reflection and dispersal of P- and S-waves.

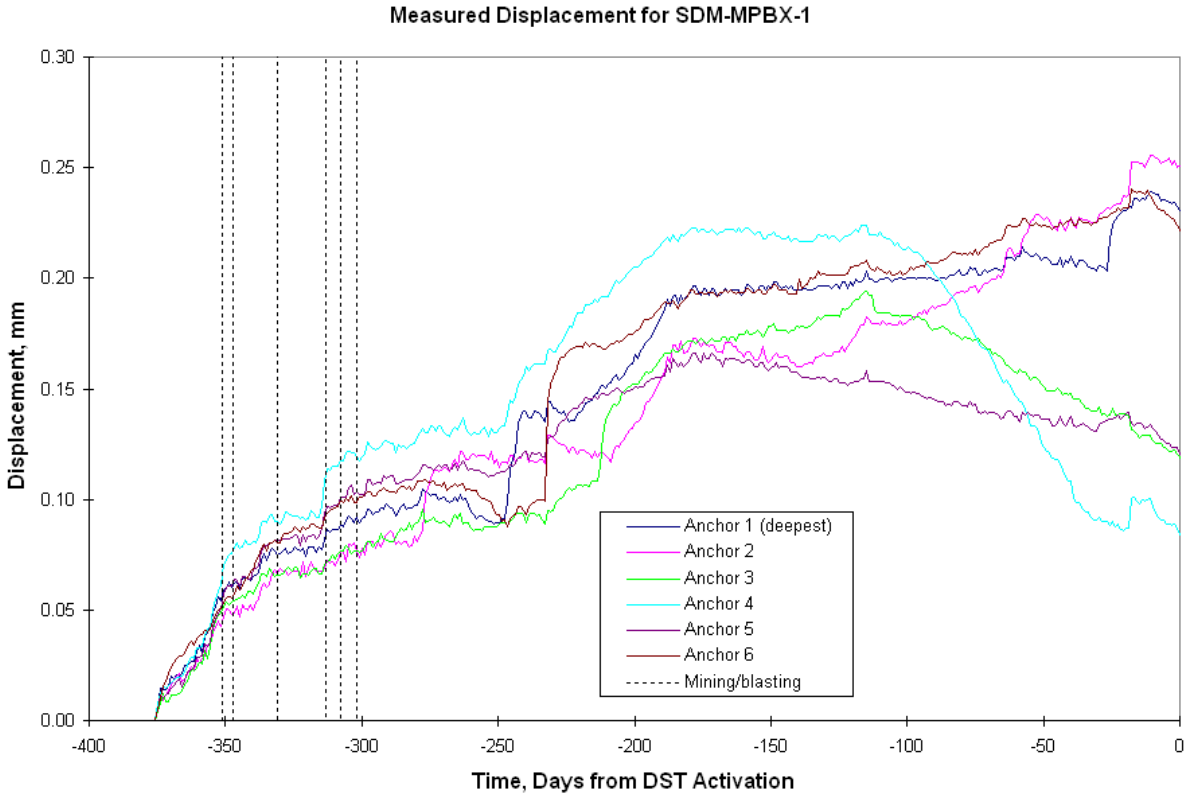

Figure 3. Measured displacements for the mine-by extensometer SDM-MPBX-1.

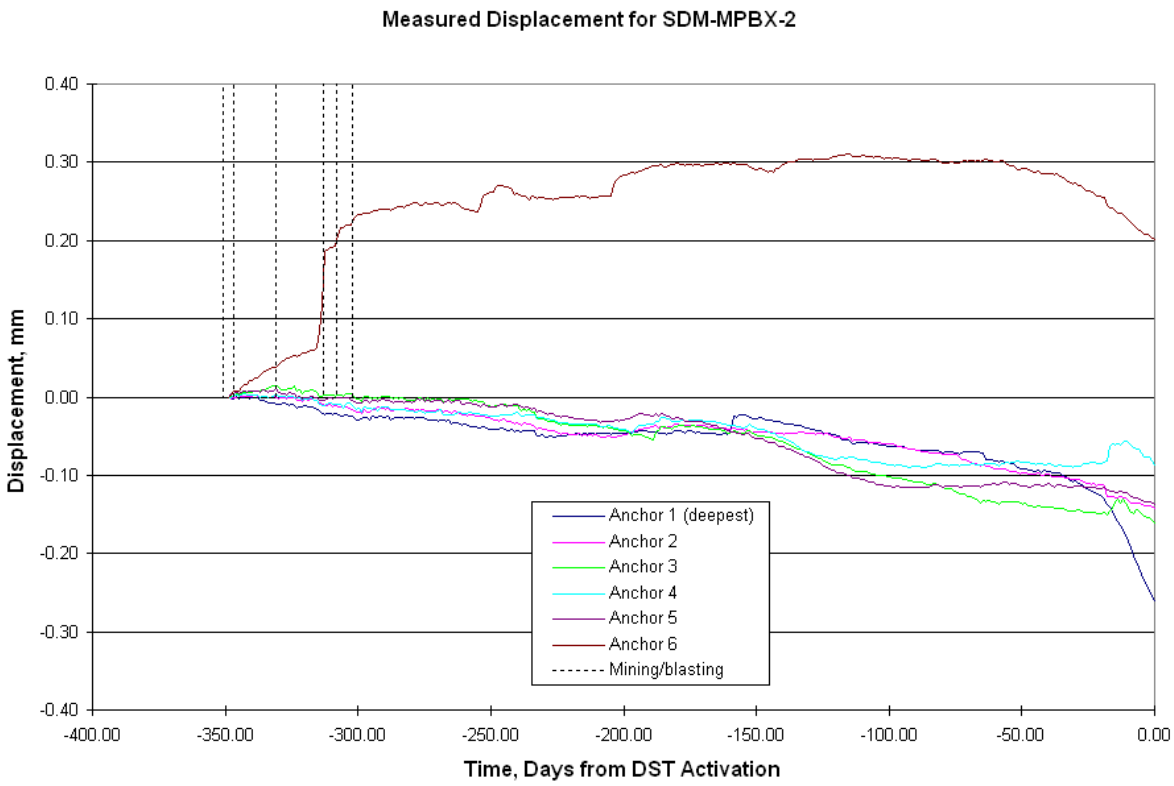

Figure 4. Measured displacements for the mine-by extensometer SDM-MPBX-2.

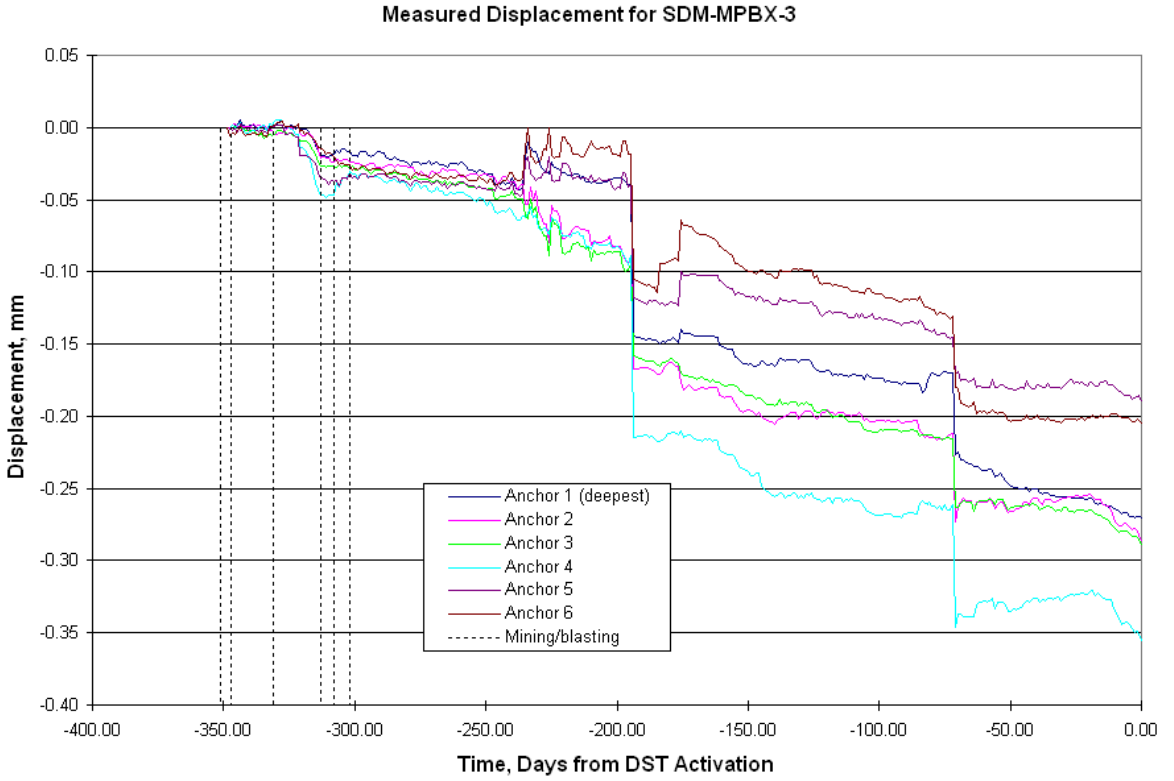

Figure 5. Measured displacements for the mine-by extensometer SDM-MPBX-3.

6. Observed damage from tunnel construction (extent of excavation damage zone (EDZ))

Several pre- and post-excavation inspections of the damage created by excavation methods were performed in the ESF (BSC, 2004; YMP, 1995; YMP, 1997a).

- The ESF was constructed using a TBM. Observations from several boreholes in the drift wall indicate that construction induced damage is confined to <0.3 m of the drift wall.
- The alcoves and heated drift were excavated using drill and blast. Excavation damage was observed primarily up to 1 m from the wall, with no damage beyond 1.5 m.
- From Tsang et al. (2004), which looked at EDZ in numerous geologic media, the EDZ was predicted to be <0.1 m for TBM tunnel, with increase in axial permeability k of ~1 om (order of magnitude), and for drill-and-blast, <0.75m thick, increase in k ~2-3 om. A 2-om increase in permeability correlates to about 10-20% decrease in rock mass modulus.
- For all YMP info and from Tsang et al., if new fractures form they tend to be parallel to tunnel (in axial direction), with negligent effect on radial fractures. Figure 3 shows photographs of a borehole in the ESF, showing the formation of a fracture parallel to the drift wall. Therefore, changes to rock mass modulus will be anisotropic.

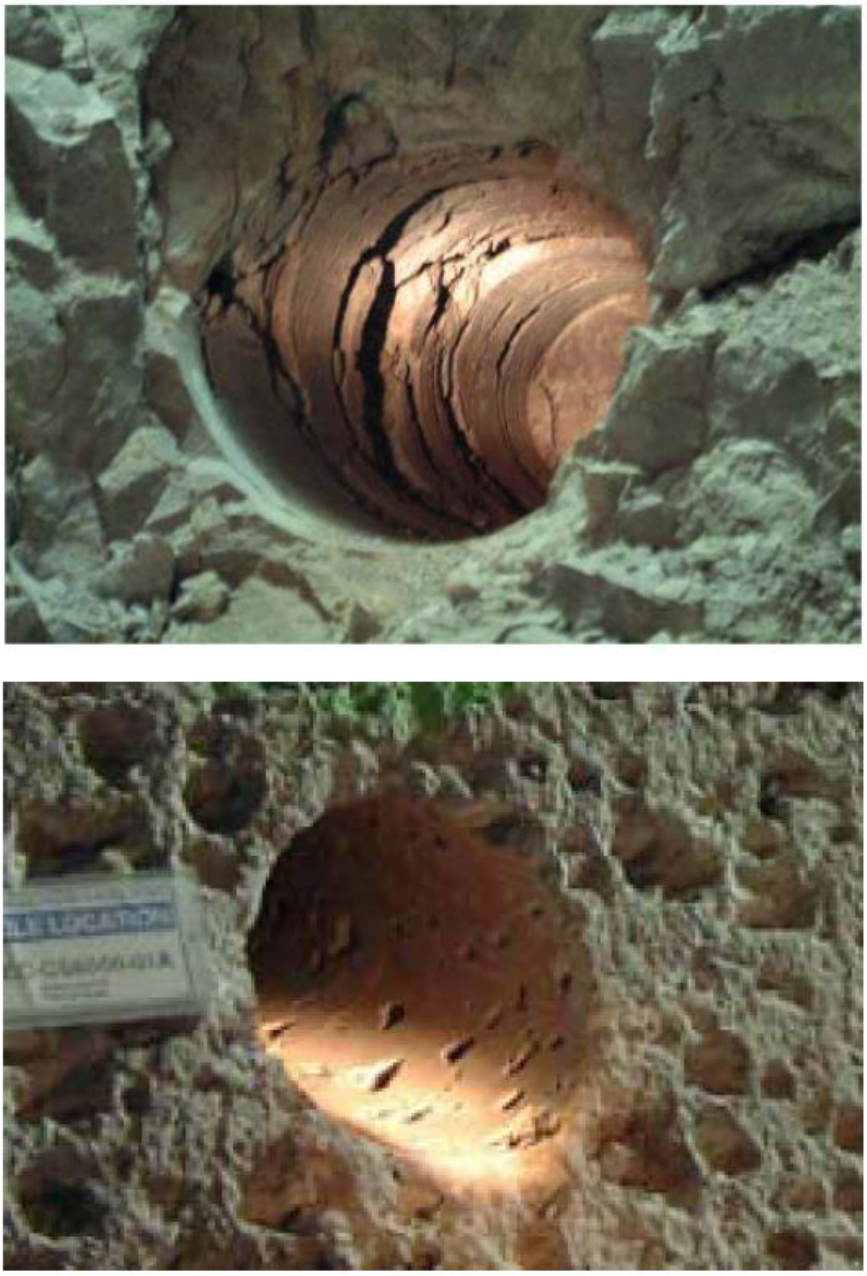

NOTE: Top photo shows sidewall fracturing/opening of preexisting wall-parallel fractures in a 12" diameter horizontal borehole drilled in the springline of the ESF in low quality Tptpll (approximately Category 1). Overburden depth is approximately 325 m. Depth of fracturing is approximately 1.5 to 2 ft (0.46 to 0.61m). The bottom photo shows a horizontal, 12-in diameter borehole drilled in the springline in good quality Tptpul (approximately Category 5) in ESF near site of slot test 2 showing no sidewall damage. The depth of overburden is approximately 250 m.

Figure 6. Observed Rock Mass Conditions at the Tunnel Springline in Lithophysal Rock in the ESF (BSC, 2004).

2.2 Tunnels in Granitic Rock

Fall and Young (1996) reported results from large-scale acoustic emission (AE) and ultrasonic-velocity monitoring studies from two tunnels used in characterization studies for potential radioactive waste disposal sites:

- The Swedish Nuclear Fuel and Waste Management Company (SKB) Äspö Hard Rock Laboratory (HRL) Äspö Island in southeastern Sweden as part of the Zone of Excavation Disturbance Experiment (ZEDEX); Two tunnels in granitic material at approximately 420 m depth, 5 m diameter, one section of tunnel was excavated using a tunnel-boring machine (TBM), while the other section was created using drill and blast techniques.
- Atomic Energy of Canada Limited (AECL) Underground Research Laboratory (URL), near Pinawa, Manitoba, Canada; mine-by tunnel in granitic material at approximately 420 m depth, 3.5 m diameter, excavated using a mechanical drilling and rock-breaking method (i.e., no blasting).

The rock type at both locations is a medium-grained granite to granodiorite. The host rock is cut by several joint sets at 420m depth, some of which are water bearing. Intact rock properties for HRL granite were taken from laboratory measurements (Ask, D., 2005):

- Static Young's Modulus of TSw2 (DST) rock – 62 GPa ± 5
- Static Poisson's Ratio 0.25 ± 0.01
- Density ~2700 kg/m^3
- Unconfined Compressive Strength ~200 MPa

A summary of the measured P-wave velocities for both sites is listed in Table 3. For all the tests, Falls and Young (1996) reported the direction of the slowest P-wave velocity was perpendicular to the tunnel wall, and the fastest P-waves were approximately parallel to the tunnel axis. The velocity-field orientation is consistent with the presence of an aligned set of microcracks parallel to the tunnel surface. This would indicate that a spalling type mechanism dominated brittle deformation in the sidewall and floor regions. Figures 7 and 8 show the measured P-wave velocity as a function of distance from the sidewall and floor, respectively, of the URL tunnel. Figure 9 plots some of the results from the ZEDEX tunnel.

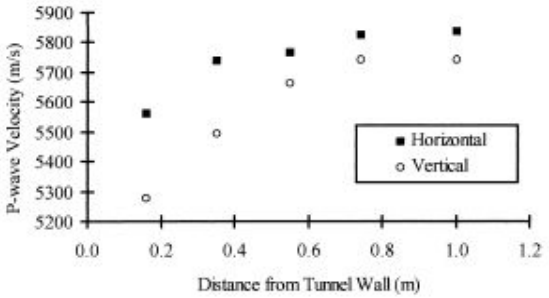

Fig. 6. P-wave velocity versus distance from the sidewall surface for ray paths tangential to the Mine-by tunnel wall (after Carlson and Young, 1993).

Figure 7. P-wave velocity measurements in the sidewall of the URL mine-by tunnel (From Falls and Young, 1996).

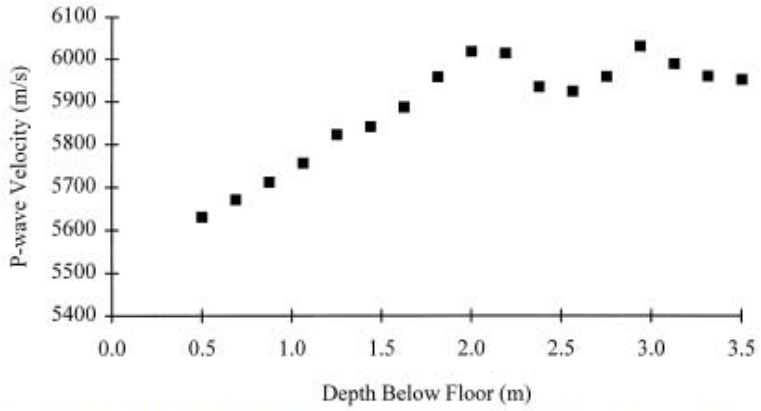

Fig. 8. P-wave velocity as a function of depth below the floor of the Mine-by tunnel. These are average velocity values corrected for anisotropy.

Figure 8. P-wave velocity measurements in the floor of the URL mine-by tunnel (From Falls and Young, 1996).

Table 3. Measured P-wave velocities at HRL and URL sites (Falls and Young, 1996).

	V_P, m/s
URL Mine-by Tunnel, Background P-wave anisotropy	
Fast	5855
Intermediate	5816
Slow	5793
HRL ZEDEX Tunnel, Background P-wave anisotropy	
Fast	6063
Intermediate	5993
Slow	5902
URL Mine-by Tunnel, Velocity field in side wall	
Fast	5695
Intermediate	5505
Slow	5065
URL Mine-by Tunnel, Velocity field in floor	
Fast	6105
Intermediate	5900
Slow	5730

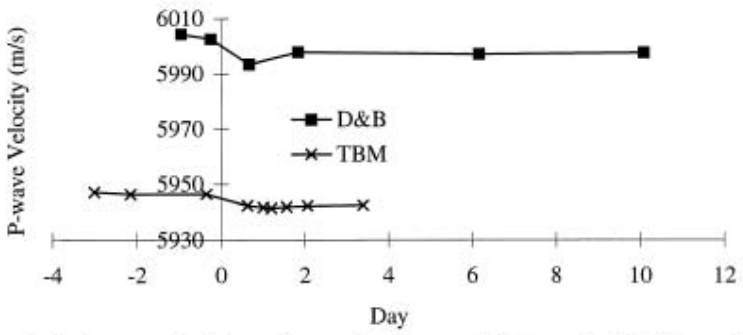

Fig. 9. Change in P-wave velocity for ray paths close to the tunnel perimeter with time as the ZEDEX tunnels were excavated through each study volume. Day zero is the time when the tunnel face passed through the centre of each sensor array. These plots are for similar orientations of the sensor arrays with respect to the D&B and TBM tunnels. Each graph starts and finishes with the tunnel face several metres on either side of the sensor array.

Figure 9. P-wave velocity measurements in the sidewall of the ZEDEX tunnel (From Falls and Young, 1996).

Falls and Young also reported observed damage from tunnel construction, and the extent of the EDZ:

- The EDZ for the URL tunnel extended out to <0.5 m of the side wall, but out to 2 m beneath the tunnel floor.
- The EDZ for the ZEBEX tunnels extended out to 0.7 m from the side wall, based on visual inspection of boreholes and P-wave velocity measurements. However, acoustic emission recording noted greater concentrations and frequency of AE events within 2 m of the drift wall, potentially indicating a lesser-damaged region to that distance. This larger excavation disturbed zone (EdZ) may exhibit higher permeability without a significant effect on rock mass modulus or P-wave velocity.

In their substantial report on rock stability considerations for the siting and construction of a repository, Martin et al. (2001) report on obtaining samples of hard rocks for laboratory testing of mechanical properties, including rock mass P-wave velocities. It was assumed that hard rocks such as granite would have very little variability as a function of depth. Typically, core samples are obtained for tunnel excavations at depths around 500 m, as opposed to in the mining and petroleum industries where samples often come from depths of several kilometers. It is generally recognized, in the petroleum industry, that softer rocks, i.e., shales, siltstones, etc., are susceptible to sample disturbance and that this process affects their laboratory properties (Santarelli and Dusseault, 1991). The process of drilling a core sample from a stressed rock mass induces a stress concentration at the sampling point. When this stress concentration is sufficient grain-scale microcracking occurs and the accumulation and growth of these microcracks ultimately leads to core disking. Martin and Stimpson (1994) showed that the accumulation of these microcracks is progressive and a function of the stress environment, i.e., increasing depth. They also showed that the accumulation of these microcracks:

- reduces the uniaxial compressive strength,
- decreases the Young's modulus,
- increases Poisson's ratio,

- increases the porosity and permeability, and
- reduces the P-wave velocity.

Of the laboratory properties examined by Martin and Stimpson (1994), the P-wave velocity showed the greatest sensitivity to sample disturbance. Figure 10 shows the comparison of the P-wave velocity measured on laboratory samples and the P-wave velocity recorded from in-situ seismic surveys. Martin and Stimpson (1994) observed a reduction in P-wave velocity of approximately 50% for granite samples taken at 1000-m depth compared to those taken at shallow depths. This change in velocity as a function of depth is not necessarily exhibited in any underground testing to date, but it may indicate that stress redistribution around a tunnel after excavation can potentially alter the seismic conductance of the host rock in the EDZ. It may also be an indicator of the change in rock mass modulus in the EDZ around a tunnel, and could be used to predict P-wave velocities in the EDZ for a tunnel at a given depth.

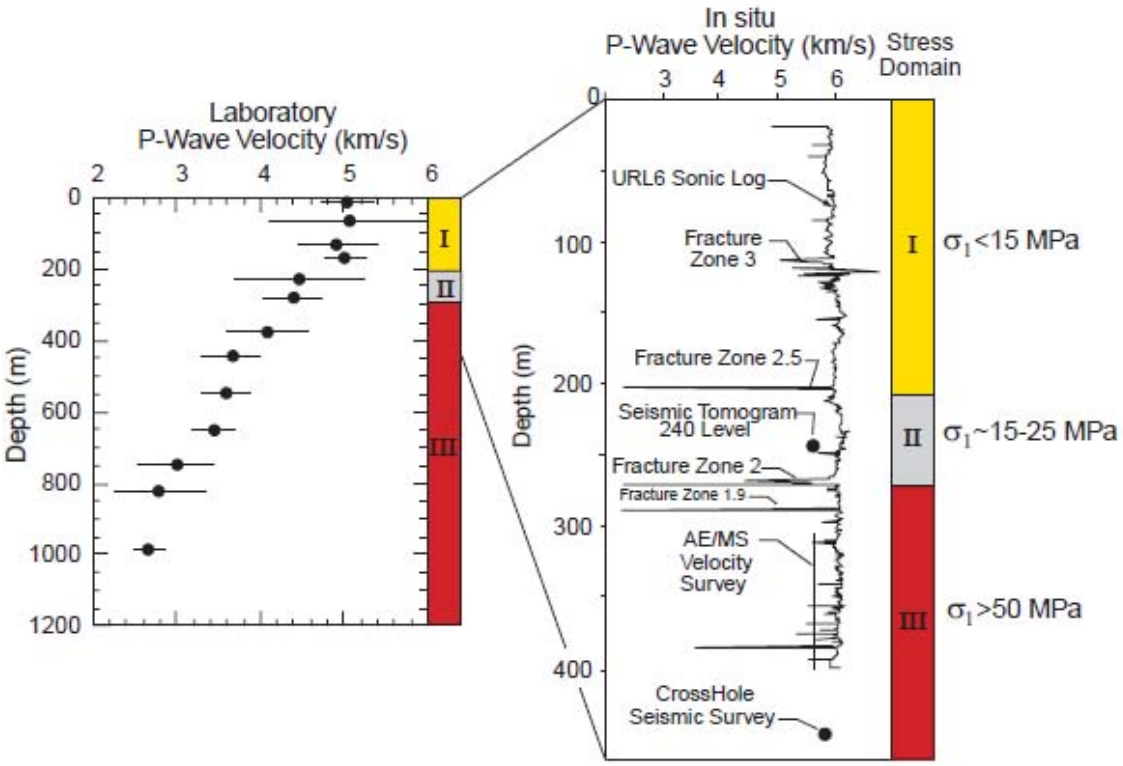

Figure 10: Comparison of the variation in P-wave velocity in laboratory samples and in-situ as a function of depth (From Martin et al., 2001, modified from Martin and Stimpson (1994)).

3. SEISMIC ANALYSIS MODEL

The technical issues concerning detecting tunnels using seismic methods are complex. While theoretically and in numerical simulations, it is expected that the distinct tunnel/wall interface would produce a reflected signal strong enough to determine the presence of a tunnel, for most instances field data fail to locate a tunnel when processed using normal methods. It is noteworthy that the reverse-time migration (RTM) method applied to field data shows promise in locating tunnels. This is because the RTM method in theory migrates the energy back to its point of origin; *i.e.*, migrates energy back to the tunnel to form an image.

Based on the characteristics of the EDZ's discussed in Section 2, it has been speculated that this damage zone scatters the seismic energy, resulting in masking of any tunnel reflection response. To assess the effects of the damage zone on seismic responses, a numerical simulation effort was undertaken. Calculations were carried out using the parallelized version of the time-domain finite-difference seismic wave propagation code developed in the Geophysics Department at Sandia National Laboratories. To minimize numerical dispersion, a spatial grid spacing of 0.25 *m* was used that allowed a maximum frequency for a Ricker wavelet of 90 *Hz*. The time step used was 0.025 *ms*. Calculations performed included a tunnel with a damage zone, a tunnel with no damage zone, and with no tunnel present.

3.1 MODEL DESCRIPTION

Properties for the Exploratory Studies Facility (ESF), the main tunnel for the Yucca Mountain Project, were used for the numerical simulations. The host earth material is Topopah Springs middle nonlithophysal tuff. The rock mass Young's modulus from Section 2.1 ranges from 11.4 *GPa* to 12.6 *GPa* with a Poisson's ratio of 0.201 and with a density of 2270 kg/m^3. The Poisson's ratio was taken from the static measurements. For the earth model, a Young's modulus of 12 GPa and a Poisson's ratio of 0.201 were used to derive a P-wave speed of 2430 *m/s* and a S-wave speed of 1480 *m/s*. Note these wave speeds agree with the in situ measurements (Section 2.1) of wave speeds of 3000 m/s for the P-wave and 1800 m/s for the S-wave. Observations from several boreholes in the drift wall indicate that tunnel construction using a tunnel boring machine induced damage that is confined to <0.3 *m* of the drift wall. Since the finite-difference operator in the code smoothes the boundaries between material property changes, for modeling purposes the damage zone thickness of 0.75 *m* was used so that there was one grid node is in the damage zone and a node on each side of the zone. To give some wave speed contrast to the host medium, in the damage zone approximately a ten percent reduction in Young's modulus was used giving the P-wave speed and S-wave speed 2340 m/s and 1430 *m/s*, respectively. A mass density of 2200 kg/m^3 was used for the damage zone. The decrease in Young's modulus for the damage zone was estimated from measured permeability increases in the damage zone. It is noteworthy that the ten percent decrease may be an over estimate. The air P-wave speed and mass density used are 350 *m/s* and 1.29 kg/m^3, respectively. Figure 11 shows the earth model used for the numerical simulations.

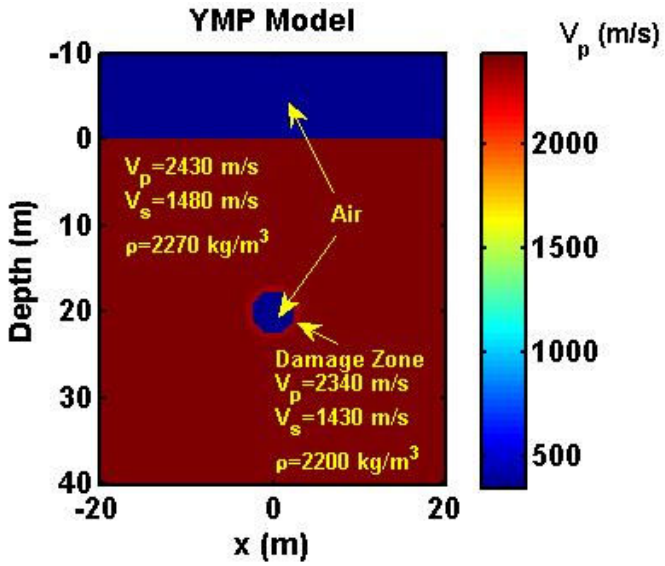

Figure 11. Earth model for seismic numerical simulations with the tunnel 20 *m* below the surface.

3.2 MODEL RESULTS

Numerical simulations were carried out using the parallel version of an in-house finite-difference elastic wave propagation code (Aldridge, 2006). All calculations were done using Sandia's high-performance computing resource REDSKY. Figure 12 shows the difference between the trace data with the tunnel and the trace data without the tunnel for the source at x=-40 *m* and the receiver string of vertical axis geophones from x=-50 *m* to x=50 *m* in 5 *m* increments. Figure 13 show similar differenced results for the source at x=-20 *m*. The seismic source is a vertical force source. Because this is differenced data, the minimum arrival time occurs near the x-position of the tunnel and not near the source.

From an examination of Figures 12 and 13, the trace responses show larger amplitudes on the positive x side of the tunnel. Tunnel is at x=0 m. In Figure 12, the differenced data for x = -15 *m* to x = 5 *m* show a different character than the other traces. In Figure 13, the difference data from x = -10 *m* to x = 5 *m* show a different character than the other traces.

Taking advantage of time slices, the unique character of the waves generated at the tunnel air-earth interface can be studied. Figure 14 shows four consecutive time slices of vertical particle motion data with tunnel minus data without the tunnel for the vertical force source at x = -40 *m*. This difference is the tunnel response. Figure 15 shows the next four consecutive time slices. Figure 16 shows four differenced time slices for the source at x=-20 *m*, which show behavior similar to Figures 14 and 15. From an examination of the time-slice data, there is a surface wave generated at the air-tunnel wall that produce waves in the host medium that then travel to the surface and sweep along the air-earth interface. These waves at the surface are measured by vertical particle motion geophones. From these simulations, the primary responses of the tunnel to a vertical seismic source are these tunnel-induced waves (much like a Stoneley wave) and not reflected or scattered responses. From the time-slice, elastic data, the damage zone does not

appear to play a significant role in the tunnel responses. The large change in the vertical particle response is at the air-damage zone interface. A very much smaller change in response occurs at the host rock-damage zone interface.

Figure 17 shows a comparison of trace data with and without the tunnel. The source is at x = -40 *m* and the receiver is at x = -30 *m*. There is a definite tunnel response as shown in the figure. The reverberations of the air in the tunnel give rise to a coda in traces measured at the surface as illustrated in Figure 18. Note that there is no coda in the background responses (no tunnel), indicating the observed coda is tunnel related and not numerical noise.

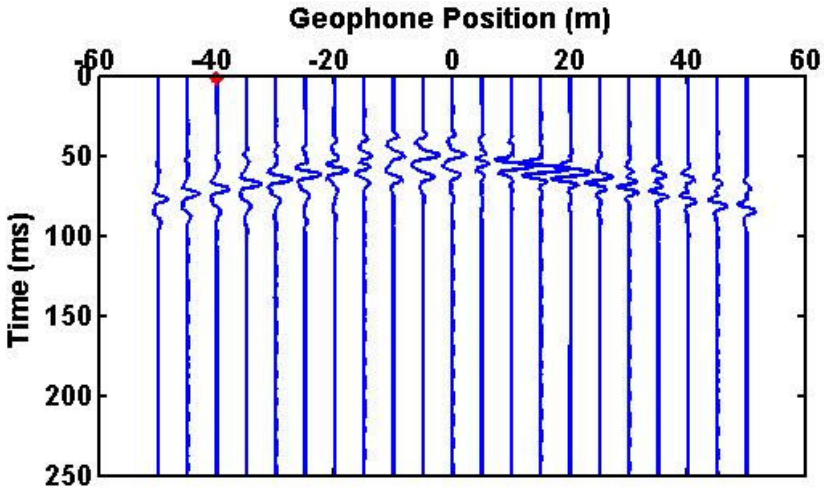

Figure 12. Trace data at the surface of the difference between responses with and without the tunnel in Figure 11. The source at x = -40 *m* is denoted by the red symbol.

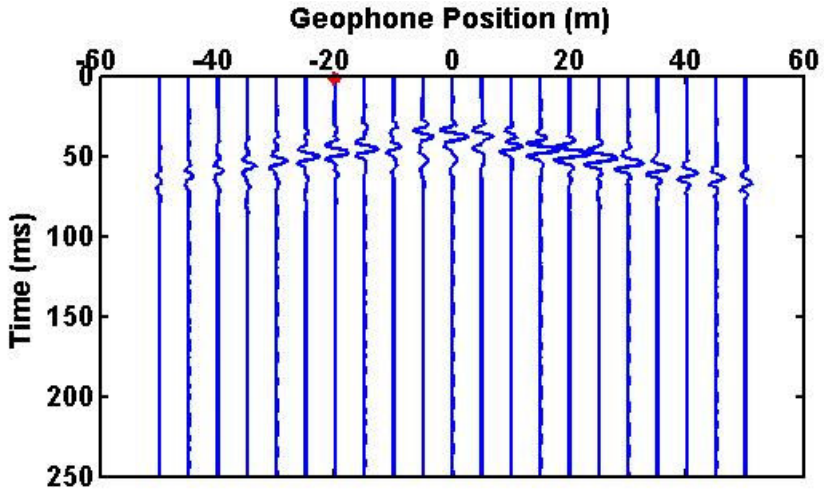

Figure 13. Trace data at the surface of the difference between responses with and without the tunnel in Figure 11. The source at x = -20 *m* is denoted by the red symbol.

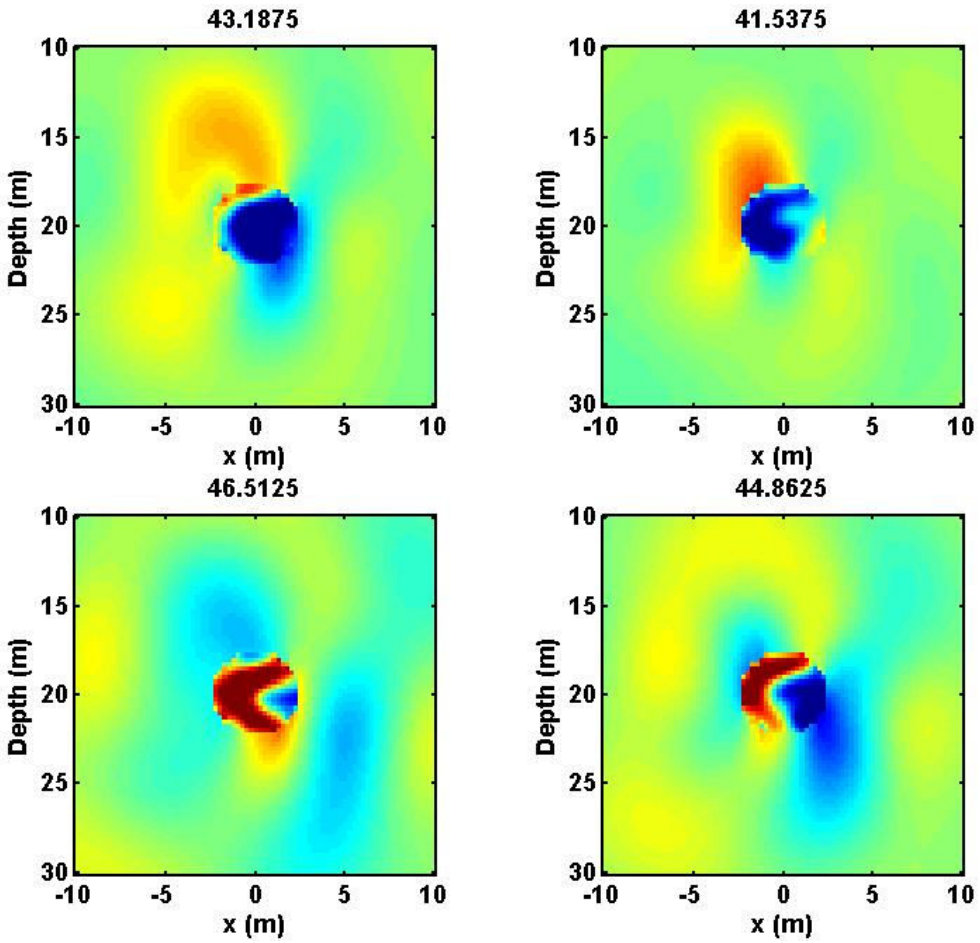

Figure 14. Four consecutive vertical particle motion time slices showing with the tunnel minus time slices without the tunnel, which displays the tunnel response. Slice titles are times in *m*s. Vertical force source is at x = -40 *m*. Warm colors are positive vertical particle motion and cool colors are negative vertical particle motion.

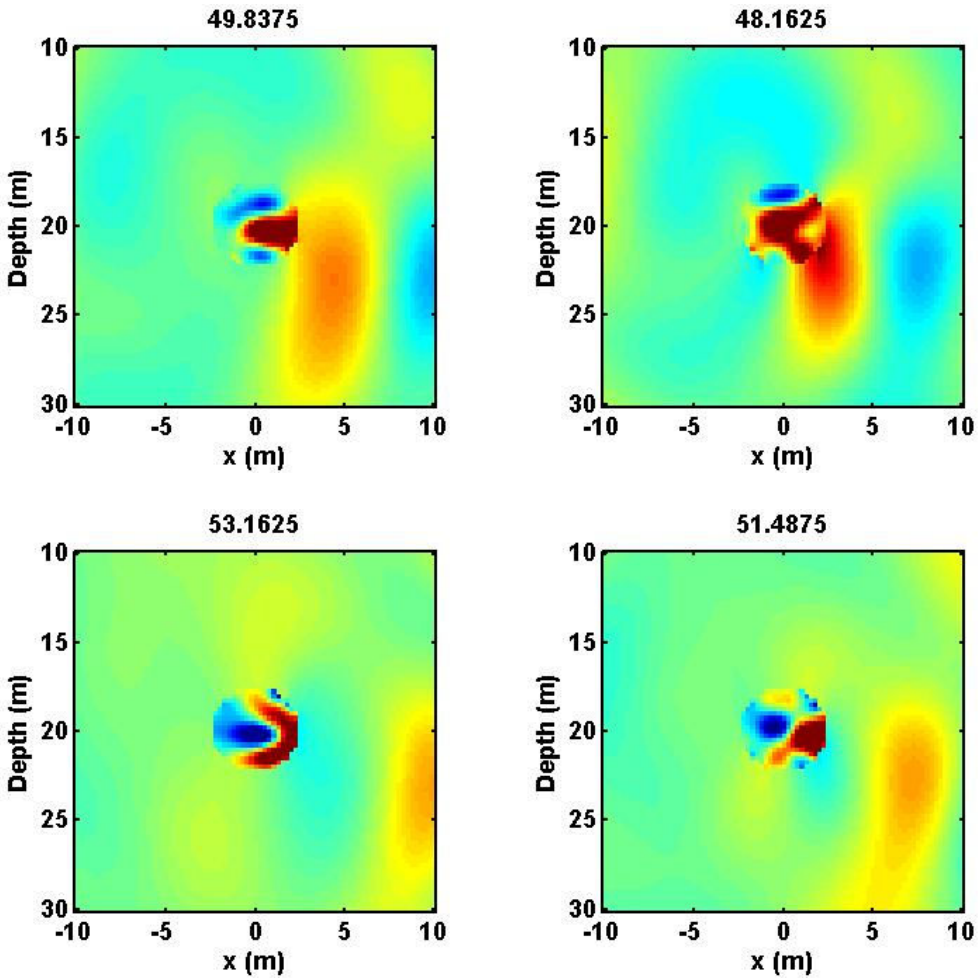

Figure 15. The next four consecutive vertical particle motion time slices following Figure 14 showing with the tunnel minus time slices without the tunnel, which displays the tunnel response. Slice titles are times in *m*s. Vertical force source is at x = -40 *m*. Warm colors are positive vertical particle motion and cool colors are negative vertical particle motion.

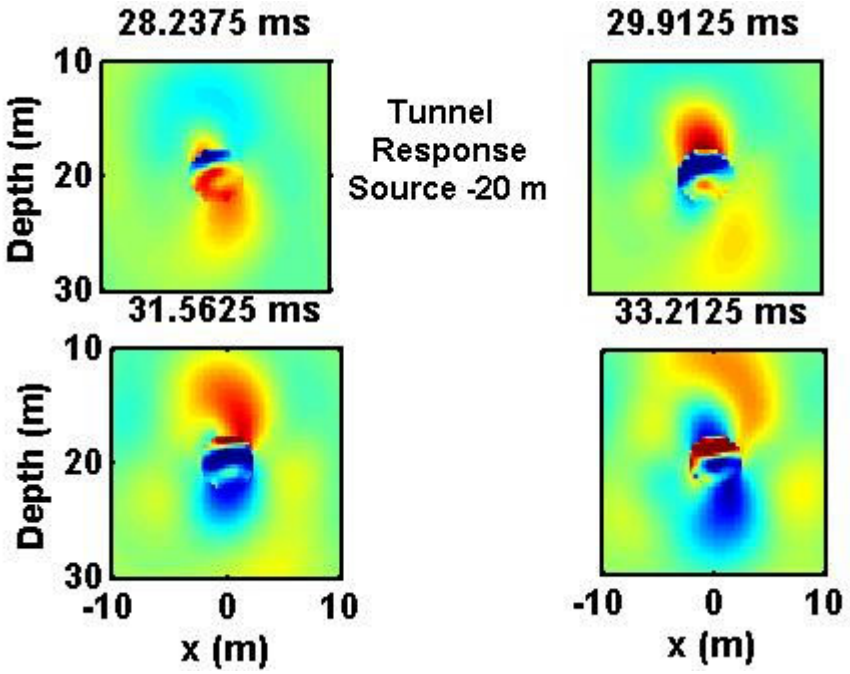

Figure 16. Time slices of with the tunnel minus time slices without the tunnel, which displays the tunnel response. Vertical force source is at x = -20 m. Warm colors are positive vertical particle motion and cool colors are negative vertical particle motion.

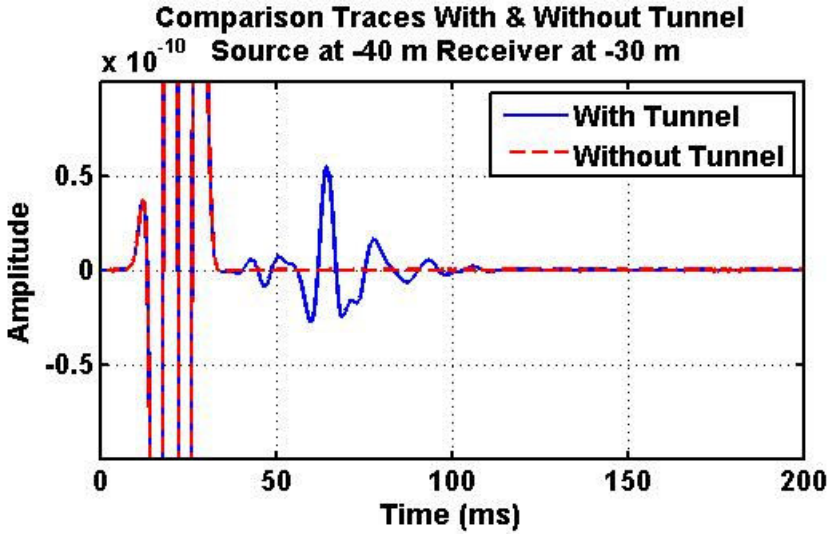

Figure 17. Comparison of trace data with and without the tunnel for the model shown in Figure 11. In this figure, the vertical force source is at x = -40 m and the receiver at x = -30 m.

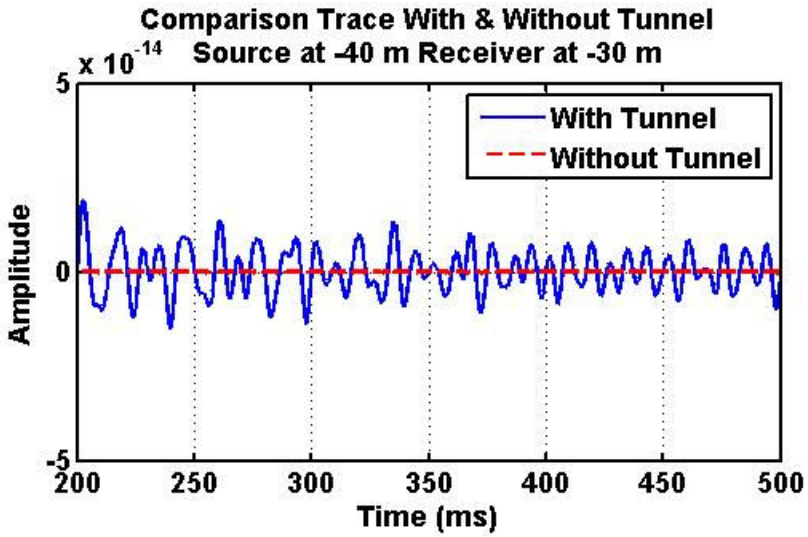

Figure 18. Comparison of the coda with the tunnel present to the absence of a coda for the background model (no tunnel present). Vertical force source is at x = -40 m and the receiver at x -30 m.

The purely elastic calculations show the ideal earth responses. To test the effects of an anelastic (attenuating) earth, numerical simulations were performed assuming quality factors Q for each wave speed regime and for both P- and S-waves. The spectral ratio is generally used for the computation of Q that relates Q to the wave amplitude, A as $1/Q = \Delta A/(\pi A)$ giving rise to an attenuation factor $\alpha = \omega/(2cQ)$ where ω is the angular frequency and c is the phase wave speed. Q does not have units. Since air in a tunnel is probably humid, a Q of 80 was assumed for air (humid air is attenuating). The anelastic model for numerical simulations is given in Table 4.

Table 4. Anelastic model for numerical simulations of tunnel responses.

Medium	V_p (m/s)	V_s (m/s)	Q_P	Q_S
Host Rock	2430	1480	80	40
Damage Zone	2340	1430	40	10
Air	350	0	80	0

Vertical particle motion time slices for the anelastic model over the time ranges Figures 14 and 15 are shown in Figures 19 and 20. The responses for the anelastic model are similar to those for the elastic model. The largest change in vertical particle motion is at the air-damage zone interface as it for the elastic model. For the anelastic model, the change in vertical particle motion at the damage zone-host rock interface is more noticeable for the anelastic case. As for the elastic case, the largest tunnel responses are from the waves produced by the surface wave at the air-damage zone interface and not from reflections or scattering from the tunnel. Figure 21 compares the trace data with and without Q for the tunnel present where the source is at x = -40 m and the receiver is at x = -30 m. Figure 22 shows and expanded version of Figure 21 to show the tunnel response in the trace data. No background response was subtracted for Figures 21 and 22. The comparison of the codas for the elastic and anelastic models is shown in Figure 23. The Q model results are similar to the elastic case except amplitude is smaller and the Q model does

not reproduce the high frequency content of the elastic cases. The amplitude of the coda with an attenuating air slowly decreases as a function of time.

A final comparison of models was done between the elastic case with and without the damage zone. At the modeled frequencies and damage zone thickness, only insignificant differences were seen between the tunnel responses in these two cases. This indicates that the damage zone would need to be much thicker or of a much greater velocity contrast to have any significant effect on the delectability of the tunnel.

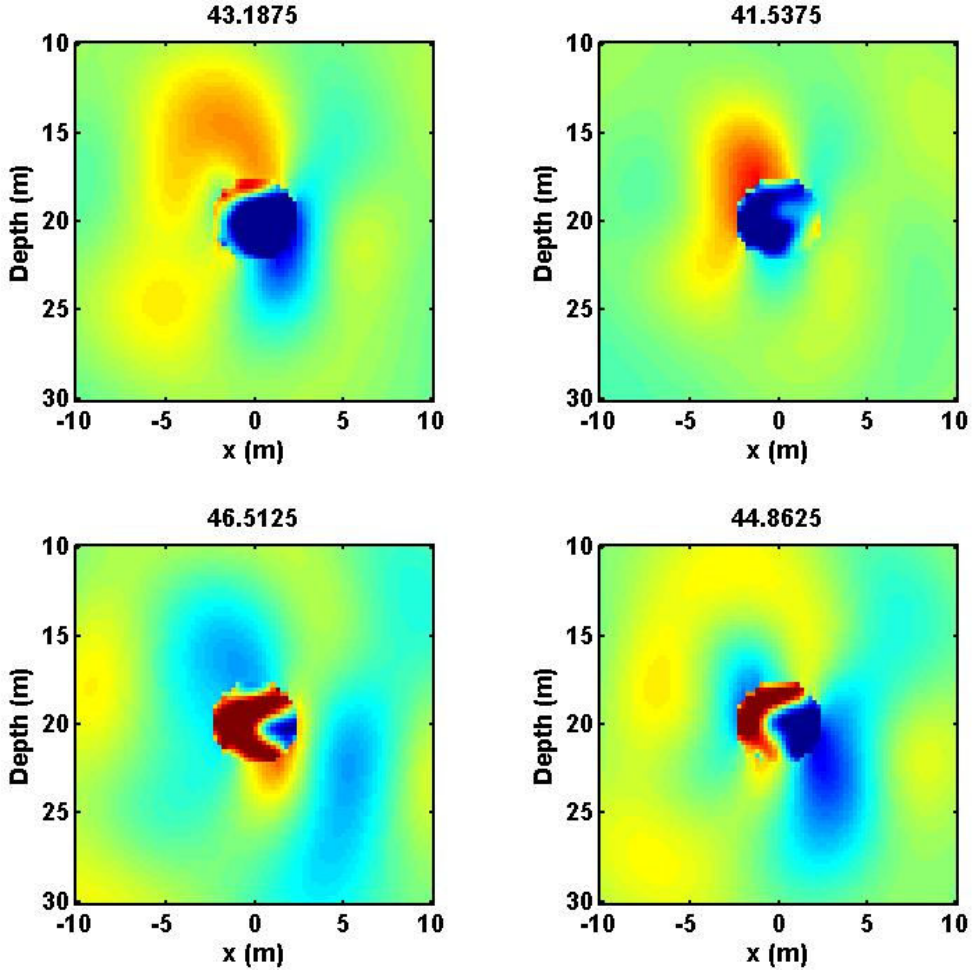

Figure 19. Vertical particle motion time slices for the anelastic earth model given in Table 4. Vertical force source at x = -40 *m*. Times are in *ms* and correspond to those in Figure 14. Warm colors are positive vertical particle motion and cool colors are negative vertical particle motion.

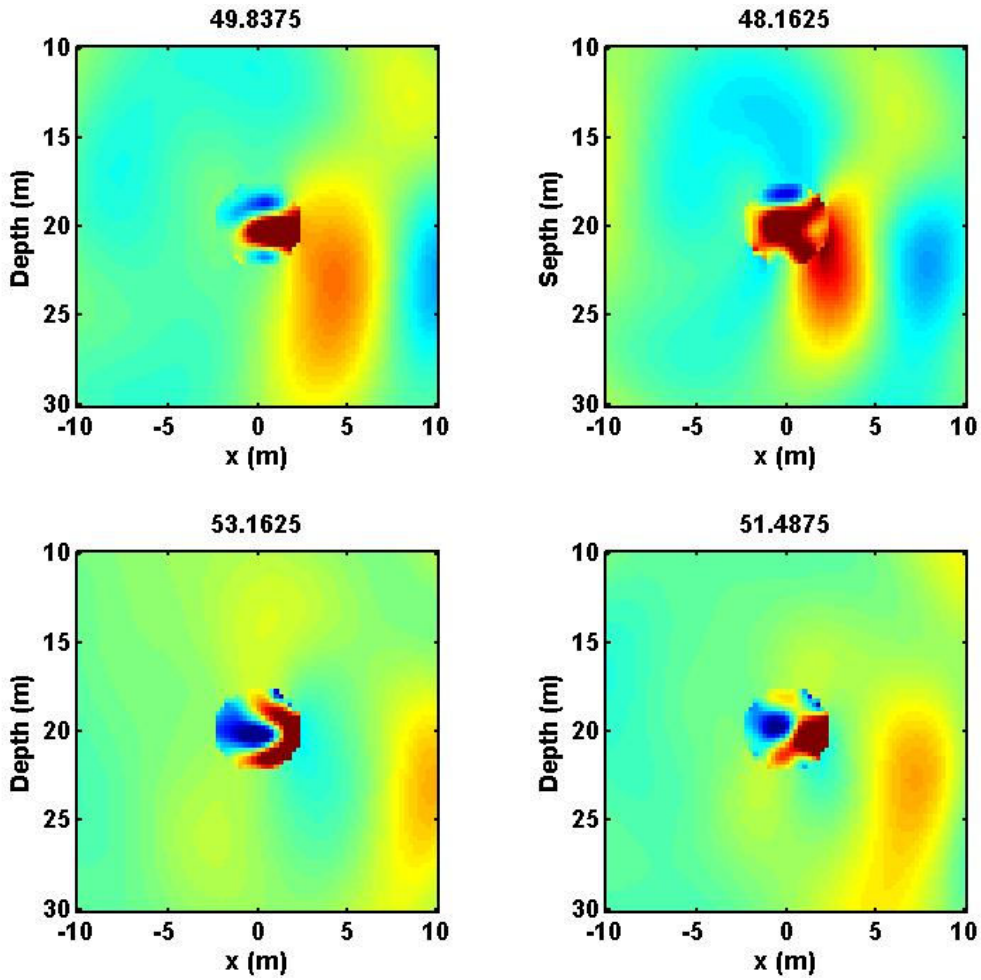

Figure 20. Vertical particle motion time slices for the anelastic earth model given in Table 4. Vertical force source at x = -40 *m*. Times are in *ms* and correspond to those in Figure 15. Warm colors are positive vertical particle motion and cool colors are negative vertical particle motion.

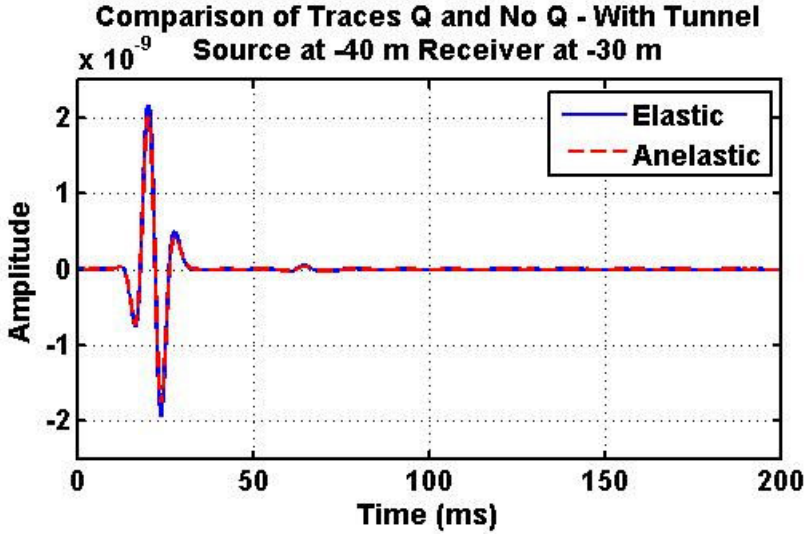

Figure 21. Comparison of vertical particle motions for the elastic (no Q) and the anelastic (with Q) models. Source at x = -40 *m* receiver at x = -30 *m*.

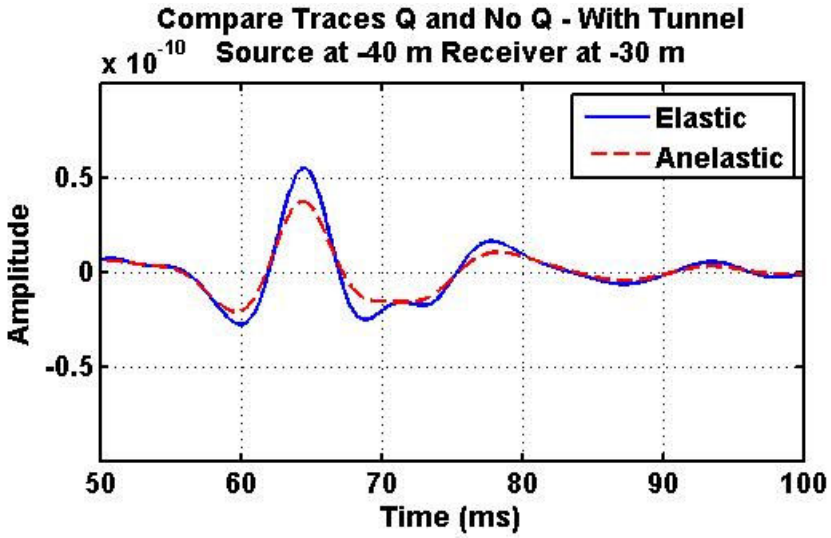

Figure 22. Expanded version of Figure 21 to show the tunnel response. Background was not subtracted from the trace data.

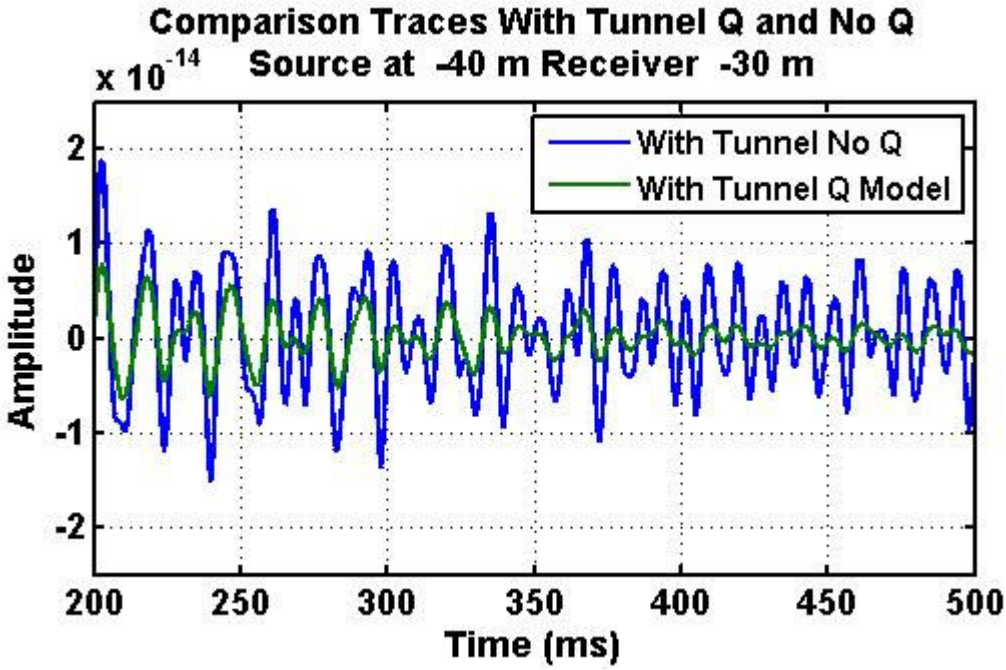

Figure 23. Comparison of the codas for the elastic model and the anelastic model. Source at x = -40 m receiver at x = -30 m.

Since the largest seismic responses are not reflections, data processed by the usual reflection method may not produce detectable tunnel responses. The largest responses are the waves produced by surface waves at the air-damage zone interface. Utilization of reverse-time migration (RTM) should image the tunnel, since in theory the method migrates the energy back to its source – the tunnel. For a discussion of reverse-time migration, the reader is referred to Bartel, *et al*., (2008). To image the subsurface, the RTM method utilizes the wavefields that are generated by a seismic source and captured by a set of receivers. The measured responses at the

receivers consist of direct arrival responses and for this application, tunnel responses. The traces measured by the receivers are time-reversed and these time-reversed traces are the input waveforms for the receivers acting as sources in a numerical simulation. Here the receivers are vertical particle motion geophones, the receivers acting as sources are then vertical force sources However, before the traces are time-reversed and played back into the background model, the direct arrivals are generally removed so that only the desired responses are used for the RTM input waveforms. These time-reversed trace input waveforms applied to the receivers acting as sources produce a time-reversed wavefield that propagates into the background model. For the seismic wave propagation, we use a 3D finite-difference elastodynamic algorithm that solves the velocity-stress system of partial differential equations (Aldridge, 2006). A critical part of the RTM process is an imaging condition; *i.e*., a methodology to produce an image using the time-reversed wavefield. One imaging condition is to take the zero-lag cross-correlation between the time-reversed wavefield emanating from the receivers acting as sources with the source wavefield collapsing onto the source. (Note that one could just as well cross-correlate a collapsing time-reversed wavefield with an expanding source wavefield.) These two wavefields are like two ships passing in the night and have a maximum in the zero-lag cross-correlation when these two wavefields (two ships) are coincident at the source of the measured response in time and hence depth. To apply the RTM process requires a background velocity model for the computation of the time-reversed wavefield and the source wavefield; therefore, the image is only as good as the background velocity model. Generally, a uniform or smoothly varying model of wave speeds and mass density is used.

The RTM method was applied to image the tunnel. The background trace data (no tunnel) was subtracted from the trace data with the tunnel present as illustrated in Figures 12 and 13. In all there were 17 actual sources along the x-axis from x = -40 m to x = 40 m at 5 m increments. There were 21 actual receivers along the x-axis from x = -50 m to x = 50 m in 5 m increments. For each actual source, a cross-correlation image was formed over a 2×2×2m grid of points. The final image is formed by adding all the individual images (17 in all). The final image along the x-axis is shown in Figure 24. An image of the tunnel is formed at x = 0 and depth ~20 m agreeing with the model show in Figure 11. There are near surface migration artifacts. The cross-correlation low (a negative value) at a depth of ~13 m is a typical tunnel response for the cross-correlation high (positive value) at a depth of 19 m.

Coda wave interferometry (*e.g*. see, Sneider, 2002) is a technique for monitoring changes in the media over time using elastic waves. Elastic waves traveling through a medium are scattered multiple times by heterogeneities in the medium and generate slowly decaying (late arriving) wave trains), called coda waves. Despite their noisy and chaotic appearance, coda waves are highly repeatable such that if no change occurs in the medium over time the waveforms are identical. If a change occurs, such as a crack, expanding damage zone, *etc*., the change in the multiple scattered waves will result in an observable change in the coda. In the case here, the major change in the coda is between traces for a tunnel present and no tunnel present, as shown in Figure 18. It is noteworthy that the modeling shows very little change in the coda between having a damage zone and no damage zone. This is because the coda is primarily produced by the acoustic reverberations in the air-filled tunnel and not multiple scattering. Coda wave interferometry uses this sensitivity to monitor temporal changes in a medium. It is beyond the

scope of this report to delve further into utilization of coda waves for tunnel detection and characterization.

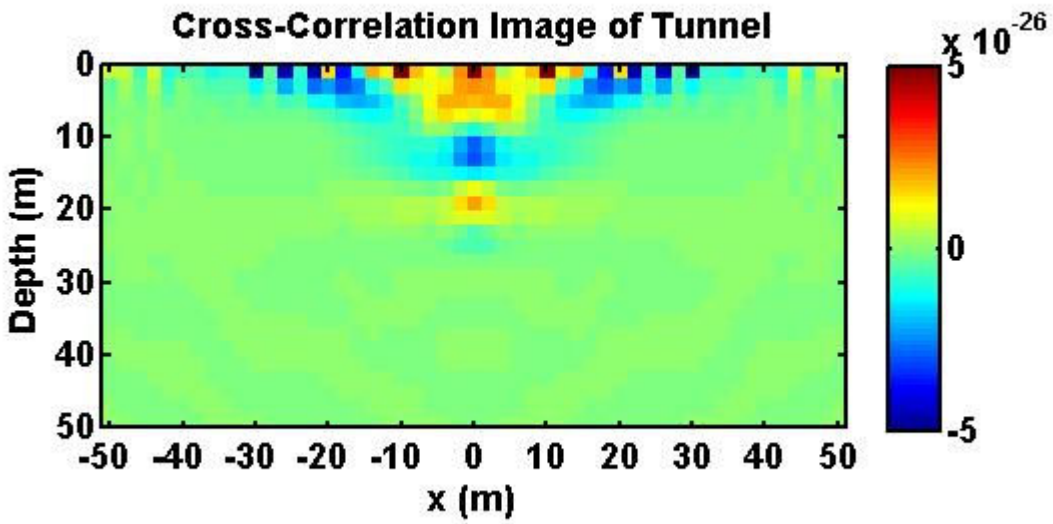

Figure 24. Cross-Correlation image of the tunnel. Center of tunnel from Figure 11 is $x = 0$ at a depth of 20 *m*. Near surface "images" are migration artifacts.

Figures 12 and 13 show trace data for the background trace data subtracted from the trace data with the tunnel to include the damage zone. The data presented in this fashion are similar to a reflection hyperbola. These types of data can be analyzed by "flattening" the hyperbola*; i.e.*, remove the moveout. The "flattened" hyperbola are shown in Figure 25 where the moveout velocities are different for the two source locations, 1410 *m/s* for source at -40 *m* and 1810 *m/s* for source at -20 *m*. The moveout velocity can be determined from the equation for the reflection hyperbola $v_m^2 t_p^2 / 4h^2 - x^2 / 4h^2 = 1$, where v_m is the moveout velocity, h is the depth to the tunnel ("reflector"), x is the position of the receivers in a line, and t_p is the first arrival time pick of the traces in Figures 12 and 13. The time shift applied to the traces is $t_s = x / v_{moveout}$, where here $v_{moveout}$ is the mean of the moveout velocity. As the source approaches the point over the tunnel, the moveout velocity increases so that over the tunnel the mean of the moveout velocity is 2370 *m/s*, which approaches the P-wave velocity of 2430 *m/s* for the model. Since the moveout velocity depends on the source-tunnel horizontal displacement, data analysis in the usual manner is not applicable. However, by determining the moveout velocity for each source location, the tunnel will be under the source with the moveout velocity nearest the P-wave velocity or at least with the maximum moveout velocity. From the moveout velocities, the location of the tunnel can be determined.

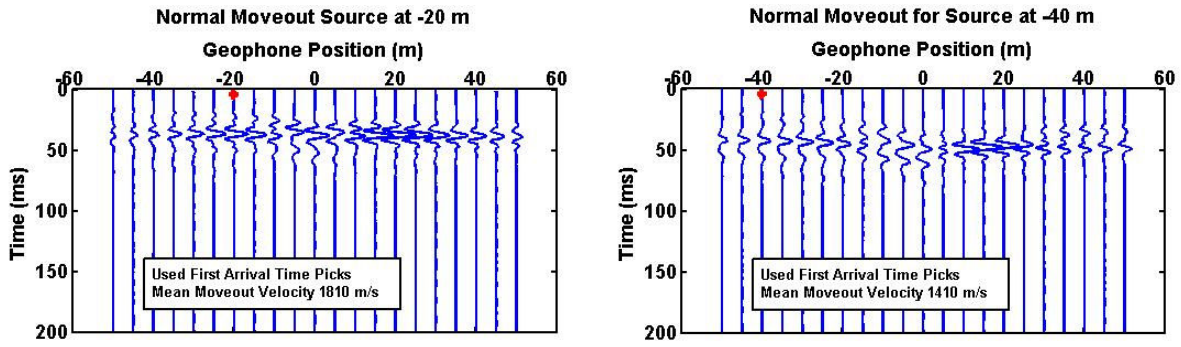

Figure 25 Moveout corrected differenced traces for sources at -40 m and – 20 m. The mean moveout velocities are 1410 *m*/*s* for source at -40 *m* and 1810 *m*/*s* for source at -20 *m.*

4. CONCLUSIONS

Mechanical and observational data developed from a potential site for disposal of radioactive waste indicate that an EDZ of at least 1m, perhaps as high as 2m, exists around excavated tunnels. The EDZ is significantly smaller for tunnels excavated using a tunnel boring machine than with alpine miners or drill-and-blast techniques. Fracture formation tends to be anisotropic, with preferential fracture formation occurring parallel to the tunnels. The decrease in P-wave velocity in the EDZ in granitic rock, as determined from either seismic velocity measurements, is approximately 10%; in volcanic tuff, the decrease is 33%, as determined from an in situ measurement of rock mass modulus. The magnitudes of these changes, and the extent of the EDZ in to the host rock, were postulated to be enough to affect measurements used for tunnel detection.

Unexpectedly, the numerical simulation of a tunnel response using YMP data for the tunnel size, damage zone, and the host rock showed an unusual behavior. Firstly, the damage zone does not appear to have much of an effect upon the tunnel response either for the purely elastic case or the anelastic case. Simulations modeling the tunnel with and without a damage zone showed almost no difference in wave behavior and therefore cannot be masking the tunnel response for tunnels of these scales and typical seismic imaging frequencies. For an EDZ with a 33% decrease in Young's modulus, the wave forms measured at the surface are the same as the wave forms for the approximately 10% reduction in Young's modulus. Secondly, for a vertical force source at the surface, the tunnel responses are waves produced or spawned by the surface waves at the air-damage zone interface, rather than pure P-wave reflections as generally thought. These spawned waves travel to the surface and sweep along the air-earth interface. Since the largest responses are not reflections, data processed in the usual way using P-wave velocities may not properly image the tunnel. One way around this is to use the RTM method, which migrates the wavefield energy back to its source and therefore should image the tunnel. RTM was used to form a cross-correlation image of the tunnel. In this image there are shallow migration artifacts.

For any source location, subtracting the background response from the tunnel response for each receiver along a line results in a hyperbola similar to that obtained in seismic reflection data of a horizontal layer. For field data, this subtraction becomes problematic where a background model has to be estimated to obtain background responses numerically. The peak in the hyperbola is at a location near the surface projection of the tunnel. Using first-break travel times, the moveout velocity that flattens the hyperbola depends upon the horizontal source-tunnel distance. The moveout velocity is a maximum where this horizontal distance is zero and is approximately the P-wave velocity. For source locations that increase the horizontal source-tunnel separation, the moveout velocity decreases. Using these apparent reflection hyperbolas may be a way to determine the horizontal location of a tunnel.

The codas of the surface measured responses are due to the presence of the tunnel and not numerical noise. Anelastic numerical simulations were performed to determine if a low Q damage zone would have an effect. From the simulations, it does not appear to affect the nature of the produced (spawned) waves, only the amplitude. The attenuation of the waves in the tunnel

air affects the coda wave. A direction of future research should be to utilize coda wave interferometry for tunnel detection and characterization.

In summary, the conclusions drawn from the observations simulations in this report are: 1) the observed EDZ is at most 2 *m* from the tunnel wall, significantly less than previously thought; 2) the presence of the damage zone has negligible effect on the waves generated at the tunnel/air interface; and 3) the assumption of P-wave reflections as the primary wave phenomenon is incorrect, and that the wave form is a spawned wave developed along the tunnel/air interface. These analyses specifically evaluated tunnels in good quality rock, for which excavation effects do not propagate great distances in the host rock. The EDZ analyses also evaluated tunnels at several hundred meters below the surface, which implies the use of low frequency seismic wave pulses at the surface, whose wavelengths are larger than the tunnel diameter. Therefore, several potentially important variables were not evaluated: 1) the potential dewatering of the region around a tunnel on wave behavior; 2) the predicted behavior for tunnels in poor quality rock, which may enhance the extent and effect of the EDZ; and 3) tunnels at shallower depths, which would allow the use of higher frequency waves which may be more affected by the presence of the EDZ.

5. REFERENCES

- Aldridge, D. F., 2006. Finite-difference numerical simulation of 3D seismic wave propagation. SAND2006-4302P, Sandia National Laboratories, Albuquerque, New Mexico.
- Bartel, L. C., D. F., Aldridge, N. P., Symons, and M. M., Haney, 2008. *Reverse-time seismic and acoustic wave propagation – high-fidelity subsurface imaging*. SAND2008-0169, Sandia National Laboratories, Albuquerque, New Mexico.
- Bechtel SAIC Company (BSC), 2002. *Thermal Testing Measurements Report*. ANL-NBS-HS-000041 REV 00, Las Vegas, Nevada, MOL.20021004.0314.
- Bechtel SAIC Company (BSC), 2004. *Drift Degradation Analysis*, ANL-EBS-MD-000027 REV 03, Las Vegas, Nevada.
- Carlson, S.R., Young, R.P., 1993. Acoustic emission and ultrasonic velocity study of excavation-induced microcrack damage at the Underground Research Laboratory. Int. J. Rock Mech. Min. Sci. Geomech. Abstr. 30, 901–907.
- Descour, J.M., K. Hanna, D. Conover, and B. Hoekstra, 2001. *Seismic Tomography Technology for the Water Infiltration Experiment*, TDR-EBS-MD-000017 REV 00, prepared for U.S. Department of Energy, Yucca Mountain Project.
- DOE (United States Department of Energy), 2007. "Strategic Petroleum Reserve Plan – Expansion to One Billion Barrels," Submitted to Congress Pursuant to the Energy and Conservation Act, as Amended. United States Department of Energy, Office of Petroleum Reserves, Washington, D.C., June 2007**.**
- Falls, S.D., and R.P, Young, 1996. "Acoustic emission and ultrasonic-velocity methods used to characterize the excavation disturbance associated with deep tunnels in hard rock," Tectonophysics 289 (1998), Elsevier Science, 1–15.
- Lin, M., L. Gilbride, M.P. Hardy, and S.R. Sobolik, 1995. *Review and Evaluation of Rock Mass Properties Modeling Techniques*, SAND95-1760, Sandia National Laboratories, Albuquerque, New Mexico.
- Martin, C. D., R. Christiansson, and J. Söderhäll, 2001. *Rock stability considerations for siting and constructing a KBS-3 repository*, Technical Report TR-01-38, Swedish Nuclear Fuel and Waste Management Company, Stockholm, Sweden.
- Martin, C. D. and B. Stimpson, 1994. The effect of sample disturbance on laboratory properties of Lac du Bonnet granite. *Can. Geotech. J.*, **31**(5):692–702.
- Santarelli, F. J. and M. B. Dusseault, 1991. Core quality control in petroleum engineering. In *Proc. 32nd U.S. Symp. on Rock Mechanics,* Norman (Ed. J.-C. Roegiers), pp. 111–120. A.A. Balkema, Rotterdam.
- SKB, 1996. *ZEDEX – A study of the zone of excavation disturbance for blasted and bored tunnels*, Technical Report SKB ICR-96-03, Vol. 1-3, Swedish Nuclear Fuel and Waste Management Company, Stockholm, Sweden.
- Sneider, R., 2002. Coda wave interferometry and the equilibration of energy in elastic media: Phys. Rev. E, **66**, 046615 1-8.
- Tsang, C-F, F. Bernier, and C. Davies, 2005. Geohydromechanical Processes in the Excavation Damaged Zone in Crystalline Rock, Rock Salt, and Indurated and Plastic Clays,

International Journal of Rock Mechanics and Mining Sciences, Volume 42, No. 1, Pages 109-125, January 2005.

- Wagner, R.E., et al., 2002, *Thermal Test Measurements Report*, YMP report ANL-NBS-HS-000041 REV00A.
- Yucca Mountain Project (YMP), 1995. Assessment of Blasting Damage in Alcove 2, DTN: SNF31120393001.004, submitted September 29, 1995, MOL.19960701.0162.
- Yucca Mountain Project (YMP), 1997a. Blast Vibration Monitoring in the Thermal Testing Facility/Connecting Drift and Heated Drift. DTN: SNF37100195001.003, submitted April 22, 1997, MOL.19971111.0208.
- Yucca Mountain Project (YMP), 1997b. Unconfined Compression Tests on specimens from the Drift Scale Test Area of the Exploratory Studies Facility at Yucca Mountain, Nevada. DTN: SNL02100196001.001, submitted May 1997.
- Yucca Mountain Project (YMP), 1997c. Thermal Expansion and thermal Conductivity of Test Specimens from the Drift Scale Test Area of the Exploratory Studies Facility at Yucca Mountain, Nevada. DTN: SNL2208196001.001, submitted May 1997.
- Yucca Mountain Project (YMP), 2000. PLT (2000) Displacement and Pressure Data. DTN: SN0011F3912298.022, submitted November 2000.
- Yucca Mountain Project (YMP), 2003. PLT (2003) Displacement and Pressure Data. DTN: SN0306F3912298.048, submitted May 2003.

- **DISTRIBUTION:**

5	MS	0705	L. C. Bartel, 6913
1	MS	0705	G. J. Elbring, 6913
1	MS	0705	L. Preston, 6913
1	MS	0751	T.W. Pfeifle, 6914
2	MS	0751	S. R. Sobolik, 6914
1	MS	0701	J. A. Merson, 6910
1	MS	0899	Technical Library, 9536 (electronic copy)


Sandia National Laboratories